CrossMark

ORIGINAL PAPER

Locking-free triangular plate element using polynomial incompatible approximation for analysis of cracked thick–thin plates

Hehua Zhu · Guangchao Zhang · Yongchang Cai

Abstract In this paper, a simple locking-free triangular plate element, referred to here as the Mindlin triangular plate element with full integration (MTPF), is presented for the analysis of cracked thick–thin plates. The element employs a new specially designed incompatible meshless approximation, independent of the nodes and triangle shape, in order to define displacements for the purpose of avoiding the use of reduced/selected integration to make the MTPF locking-free and valid for the thin plate. The current MTPF is also extended for the analysis of cracked thick–thin plates, and the virtual crack closure technique is applied in order to compute the crack tip stress intensity factors of the cracked thick–thin plates, where the formula derivation and numerical implementation are very simple and convenient for the present MTPF. Several representative numerical examples demonstrate that the MTPF is a robust and high-performance element for cracked thick–thin plates.

Keywords Plate · Triangular element · Reissner–Mindlin · Meshless · Meshfree · Crack

H. Zhu · G. Zhang (✉) · Y. Cai
State Key Laboratory of Disaster Reduction in Civil
Engineering, College of Civil Engineering, Tongji
University, Shanghai 200092, China
e-mail: 1310183@tongji.edu.cn

1 Introduction

Plate (and shell) structures play an important role and offer wide applications in civil, mechanical, and aerospace engineering. The existence of defects and cracks in such structures may lead to a substantial decrease in load capacity, structural safety, and even structural collapse, and therefore, accurate evaluation of the fracture mechanics parameters of the cracked plates is an important topic in structural engineering practice.

Generally, elastic plate analysis can be performed by means of three-dimensional elasticity, Kirchhoff plate formulation, or Reissner–Mindlin plate theory (Bayesteh and Mohammadi 2011). Among these theories, Reissner–Mindlin plate theory may be the most widely used in engineering applications, because it requires only C_0 continuity for the displacement fields, avoids the C_1 continuity requirement difficulties in the Kirchhoff-type theory, and has a relatively very low computational cost compared to the three-dimensional theory. Unfortunately, the Reissner–Mindlin plate elements suffer from the shear locking phenomenon and yield poor results in a thin plate limit (Ayad et al. 1998; Cen and Shang 2015). Techniques including the assumed shear strain approach, discrete Kirchhoff/Reissner–Mindlin representation, mixed/hybrid formulation, and reduced/selected integration have been employed in order to develop the locking-free triangular thick–thin plate elements, such as the element DST-BL by Batoz and Lardeur (1989),

the element DST-BK by Batoz and Katili (1992), the element MITC by Bathe and Dvorkin (1985), the element MiSP by Ayad et al. (1998), the element DKMT by Katili (1993), the element RDKTM by Chen and Cheung (2001), and the element TIP3 by Brasile (2008). Many of these elements exhibit high accuracy, demonstrate effective performance for thick and thin plates, and are applicable to a wide range of practical engineering problems. However, these popular elements always involve very complex formulations to include the transverse shear effects, and are seldom used in the fracture analysis of cracked plates, because of their more complex mathematical patterns around the crack tip.

In recent years, several alternative computational methods or techniques have been proposed in order to solve cracked bending problems, including the three-dimensional FE method (Agnihotri and Parameswaran 2016), extended finite element method (Yu et al. 2014; Nasirmanesh and Mohammadi 2015), dual boundary element method (Dirgantara and Aliabadi 2000, 2002), phantom-node method (Chau-Dinh et al. 2012), strip yield model (Chang and Kotousov 2012), singular finite elements (Lim 2011), extended isogeometric analysis method (Bhardwaj et al. 2015, 2016), reproducing kernel meshless approach (Mohammad et al. 2011; Wang and Peng 2013; Tanaka et al. 2015), and discrete shear gap method (Nguyen-Thoi et al. 2012, 2014, 2015; Liu et al. 2015; Nguyen-Xuan et al. 2009; Phung-Van et al. 2013a, b). The majority of these methods are free of shear-locking, avoid remeshing of finite elements, exhibit high accuracy, demonstrate great potential and promising application for cracked plate modeling, and are undergoing rapid development.

In the work of Cai and Zhu (2017a, b), a simple MTP9 (Mindlin-type triangular plate element with nine degrees of freedom) was proposed for thick–thin plate analysis. The element MTP9 avoids shear locking, and exhibits an effective convergence rate as well as high accuracy; however, reduced/selected integration must still be applied to the shear energy term to make the element MTP9 valid for the thin plate. In this study, several specifically designed meshless approximations are employed for the construction of a new type of locking-free MTPF without the use of reduced/selected integration, which is necessary in the element MTP9. Moreover, the present MTPF is extended for the analysis of cracked thick–thin plates, and the virtual crack closure technique (VCCT) is employed in order to com-
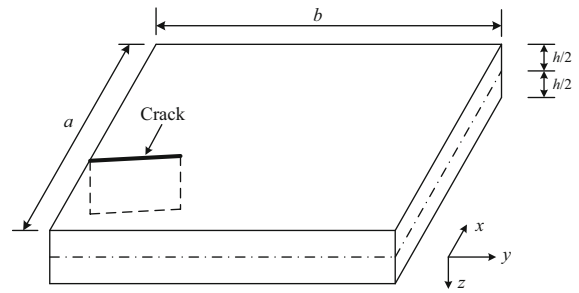
Fig. 1 Linear elastic bending plate
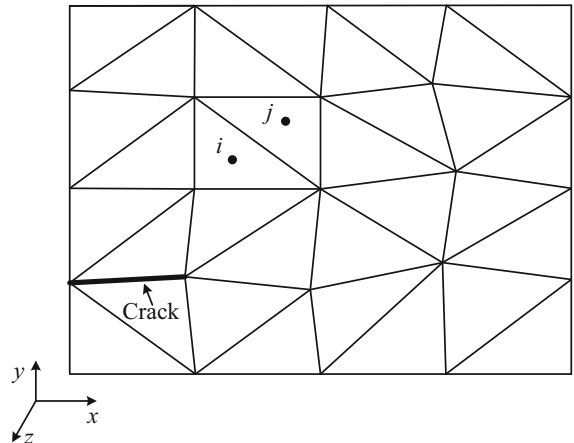
Fig. 2 Triangular mesh for mid-surface of plate

pute the crack tip stress intensity factors (SIFs) of the cracked thick–thin plates, in which the formula derivation and numerical implementation are very simple and convenient. Numerical evaluation demonstrates that the element MTPF is highly useful and applicable to practical engineering.

2 Basic theory of element MTPF

2.1 Meshless approximation at triangular element

We consider a linear elastic plate containing a through-thickness crack and undergoing infinitesimal deformation, as shown in Fig. 1. The length, width, and height of the plate are a, b, and h respectively. The plate mid plane is taken as the $x - y$ plane. The z-axis is perpendicular to the mid plane, which is divided into arbitrary triangular elements, as illustrated in Fig. 2.

According to the Reissner–Mindlin plate theory, a meshless approximation in each triangular element e_i is assumed as

$$\mathbf{u} = \mathbf{N}^e \mathbf{a}^e \tag{1}$$

where $\mathbf{u} = \{ u \ v \ w \}^{\mathrm{T}}$ is the displacement approach of e_i along the x, y, and z axes; $\mathbf{a}^e = [a_1 \ a_2 \ \cdots \ a_m]^{\mathrm{T}}$ is the interpolation degrees of freedom (d.o.f.) of e_i; $\mathbf{N}^e$ is the shape function of e_i, where

$$\mathbf{N}^e = \begin{bmatrix} z\mathbf{P}^{\mathrm{T}}(\mathbf{x}) & 0 & 0 \\ 0 & z\mathbf{P}^{\mathrm{T}}(\mathbf{x}) & 0 \\ 0 & 0 & \mathbf{P}^{\mathrm{T}}(\mathbf{x}) \end{bmatrix} \tag{2}$$

are employed in this work. Here, $x_0 = x - x_i$, $y_0 = y - y_i$, (x_i, y_i) are the coordinates of the central point of element e_i, and the linear shape function is taken as

$$\mathbf{P}^{\mathrm{T}}(\mathbf{x}) = [1 \ x_0 \ y_0]. \tag{3}$$

The quadratic shape function is taken as

$$\mathbf{P}^{\mathrm{T}}(\mathbf{x}) = [1 \ x_0 \ y_0 \ x_0^2 \ x_0 y_0 \ y_0^2] \tag{4}$$

and the cubic shape function is taken as

$$\mathbf{P}^{\mathrm{T}}(\mathbf{x}) = [1 \ x_0 \ y_0 \ x_0^2 \ x_0 y_0 \ y_0^2 \ x_0^3 \ x_0^2 y_0 \ y_0^2 x_0 \ y_0^3] \tag{5}$$

The displacement approximation in Eq. (1) is a meshless interpolation, which is defined at the central point of element e_i and is independent of the nodes and element shape. Moreover, (x_i, y_i) are the central point coordinates of element e_i. Because the displacement approximation in Eq. (1) is independent of the nodes and element shape, an arbitrary displacement approximation order, as required by the solving accuracy, can be constructed with no difficulty in the current plate element.

Substituting Eq. (1) into the following strain–displacement relations of the linear elastic problem,

$$\varepsilon_x = \frac{\partial u}{\partial x}, \ \varepsilon_y = \frac{\partial v}{\partial y}, \ \varepsilon_z = \frac{\partial w}{\partial z} \approx 0,$$
$$\gamma_{xy} = \frac{\partial u}{\partial y} + \frac{\partial v}{\partial x}, \ \gamma_{yz} = \frac{\partial w}{\partial y} + \frac{\partial v}{\partial z}, \ \gamma_{xz} = \frac{\partial u}{\partial z} + \frac{\partial w}{\partial x} \tag{6}$$

we obtain

$$\boldsymbol{\varepsilon} = \mathbf{L}\mathbf{u} = \mathbf{L}\mathbf{N}^e \mathbf{a}^e = \mathbf{B}\mathbf{a}^e \tag{7}$$

where $\boldsymbol{\varepsilon} = \{ \varepsilon_x, \varepsilon_y, \gamma_{xy}, \gamma_{yz}, \gamma_{xz} \}^{\mathrm{T}}$ is the strain vector and $\mathbf{B}$ is the strain matrix. Furthermore,

$$\mathbf{B} = \mathbf{L}\mathbf{N}^e \tag{8}$$

$$\mathbf{L} = \begin{bmatrix} \frac{\partial}{\partial x} & 0 & 0 \\ 0 & \frac{\partial}{\partial y} & 0 \\ \frac{\partial}{\partial y} & \frac{\partial}{\partial x} & 0 \\ 0 & \frac{\partial}{\partial z} & \frac{\partial}{\partial y} \\ \frac{\partial}{\partial z} & 0 & \frac{\partial}{\partial x} \end{bmatrix} \tag{9}$$

For an isotropic linear elastic material, we can express the stress–strain relations in element e_i as

$$\boldsymbol{\sigma} = \mathbf{D}\mathbf{B}\mathbf{a}^e \tag{10}$$

where the elasticity matrix

$$\mathbf{D} = D_0 \begin{bmatrix} 1 & v & 0 & 0 & 0 \\ v & 1 & 0 & 0 & 0 \\ 0 & 0 & \frac{1-v}{2} & 0 & 0 \\ 0 & 0 & 0 & \frac{1-v}{2k} & 0 \\ 0 & 0 & 0 & 0 & \frac{1-v}{2k} \end{bmatrix} \tag{11}$$

Here $D_0 = \frac{E}{1-v^2}$, E is the elastic modulus, v is the Poisson ratio, and $k = 1.2$ is the shear correction factor of the section. Because $\sigma_z \ll \sigma_x$ and $\sigma_z \ll \sigma_y$ in the Reissner–Mindlin plate theory, σ_z and its influence on deformation are neglected in Eqs. (7) and (10).

Thus, the strain energy of element e_i can be expressed as

$$\boldsymbol{\Pi}^e = \frac{1}{2} \left(\mathbf{a}^e \right)^{\mathrm{T}} \int_{-h/2}^{h/2} \left(\int\int_{\Delta e_i} \mathbf{B}^{\mathrm{T}} \mathbf{D}\mathbf{B} dx dy \right) dz \mathbf{a}^e \tag{12}$$

With the definition of the meshless approximation in Eq. (1), the adjacent elements e_i and e_j in Fig. 2 have their own d.o.f. and independent deformation, which means that these elements are totally discontinuous. However, the displacement and deformation over the share boundary of non-overlapping elements e_i and e_j should actually be continuous. A fictitious thin layer e_l may be introduced, with length l, width δ, and height h, where $\delta \ll l$ and $\delta \ll h$, in order to enforce the continuous conditions over the share boundary of the elements, as shown in Fig. 3.

Because $\delta \ll l$ and $\delta \ll h$, points p_1 and p_2 in Fig. 3 can be regarded approximately as the same point

The height of the elements along the z axis is h
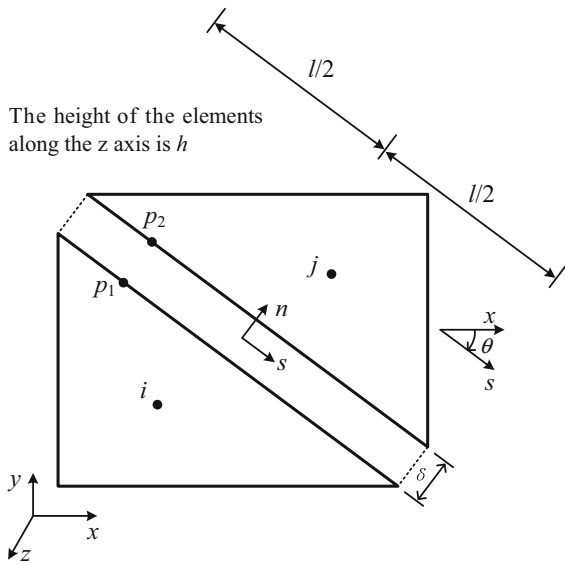
Fig. 3 Fictitious thin layer over share boundary

p, having local coordinates (s, n, z) and global coordinates (x_p, y_p, z_p), and the strain–displacement relations in thin layer e_l are simplified as

$$\gamma_{ns} \approx \frac{\bar{u}^{p_2} - \bar{u}^{p_1}}{\delta}, \varepsilon_n \approx \frac{\bar{v}^{p_2} - \bar{v}^{p_1}}{\delta}, \gamma_{nz} \approx \frac{\bar{w}^{p_2} - \bar{w}^{p_1}}{\delta} \tag{13}$$

where $\bar{\mathbf{u}}^{p_1}$ and $\bar{\mathbf{u}}^{p_2}$ can be computed using Eq. (1), as follows:

$$\bar{\mathbf{u}}^{p_1} = \lambda^l \mathbf{N}^{e_i}\left(x_p, y_p, z_p\right)\mathbf{a}^{e_i} \tag{14}$$

$$\bar{\mathbf{u}}^{p_2} = \lambda^l \mathbf{N}^{e_j}\left(x_p, y_p, z_p\right)\mathbf{a}^{e_j} \tag{15}$$

Here, $\mathbf{N}^{e_i}\left(x_p, y_p, z_p\right)$ is the shape function of point p in element e_i, $\mathbf{N}^{e_j}\left(x_p, y_p, z_p\right)$ is the shape function of point p in element e_j, $\mathbf{a}^{e_i}$ is the d.o.f. of element e_i, $\mathbf{a}^{e_j}$ is the d.o.f. of element e_j, and λ^l is the transformation matrix from the global coordinates (x, y, z) to local coordinates (s, n, z), where

$$\lambda^l = \begin{bmatrix} \cos\theta & \sin\theta & 0 \\ -\sin\theta & \cos\theta & 0 \\ 0 & 0 & 1 \end{bmatrix} \tag{16}$$

The detailed derivation process of Eq. (13) can be found in the work of Cai and Zhu (2017a). Substituting Eqs. (14) and (15) into Eq. (13) results in

$$\boldsymbol{\varepsilon}^l = \frac{1}{\delta}\mathbf{N}^l\mathbf{a}^l \tag{17}$$

where

$$\boldsymbol{\varepsilon}^l = \begin{bmatrix} \gamma_{ns} & \varepsilon_n & \gamma_{nz} \end{bmatrix}^{\mathrm{T}} \tag{18}$$

$$\mathbf{N}^l = \lambda^l \begin{bmatrix} -\mathbf{N}^{e_i} & \mathbf{N}^{e_j} \end{bmatrix} \tag{19}$$

$$\mathbf{a}^l = \begin{bmatrix} \mathbf{a}^{e_i} \\ \mathbf{a}^{e_j} \end{bmatrix} \tag{20}$$

The stress–strain relations in thin layer e_l are then expressed as

$$\boldsymbol{\sigma}^l = \mathbf{D}^l\boldsymbol{\varepsilon}^l \tag{21}$$

where

$$\boldsymbol{\sigma}^l = \begin{bmatrix} \tau_{ns} & \sigma_n & \tau_{nz} \end{bmatrix}^{\mathrm{T}} \tag{22}$$

$$\mathbf{D}^l = \begin{bmatrix} G_0 & 0 & 0 \\ 0 & E_0 & 0 \\ 0 & 0 & G_0/k \end{bmatrix} \tag{23}$$

in which $G_0 = \frac{E}{2(1+v)}$, $E_0 = \frac{E}{1-v^2}$, and $k = 1.2$. The material constants in Eq. (23) are taken as those of the average of elements e_i and e_j. The width δ of the fictitious thin layer e_l is an important artificial parameter for the MTPF, but it is easy to select a reasonable δ to satisfy $\delta \ll l$ and $\delta \ll h$ in the current formulation. Numerical studies indicate that the variation of δ in a relatively large range has little effect on the accuracy of the calculation results for the analyses of thick–thin plates in practical engineering. In this paper, the width δ is taken as $\delta = 0.0001l$.

It can be seen that, if the fictitious thin layer e_l is replaced by contact springs k_s, k_n, and k_z between adjacent elements, the current formulation becomes a discontinuous deformation analysis (DDA, Shi 1993) type of method for plate analysis, which is also a special case of the numerical manifold method (NMM, Shi 1991).

Therefore, the strain energy of thin layer e_l can be expressed as

$$\boldsymbol{\Pi}^l = \frac{1}{2\delta}\left(\mathbf{a}^l\right)^{\mathrm{T}}\int_{-h/2}^{h/2}\left(\int_{-l/2}^{l/2}\left(\mathbf{N}^l\right)^{\mathrm{T}}\mathbf{D}^l\mathbf{N}^l ds\right)dz\mathbf{a}^l \tag{24}$$

The enforcement of the displacement and load boundary conditions can be derived in a similar manner (Cai and Zhu 2017a) as in Eq. (24). Please refer to Cai and

Fig. 4 Minor adjustment at crack tip for implementation of VCCT
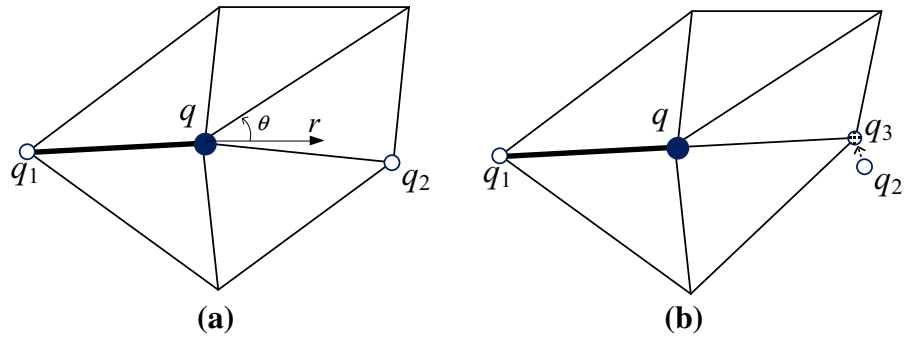
Zhu ([2017a](#)) for the detailed derivation of the equilibrium equation for the plate

$$\mathbf{K} \cdot \mathbf{U} = \mathbf{F} \tag{25}$$

where $\mathbf{K}$ is the global stiffness matrix, $\mathbf{F}$ is the force vector, and $\mathbf{U}$ is the d.o.f. vector to be solved.

It is well established that the general Reissner–Mindlin triangular plate element sharing degrees of freedom at the nodes exhibits the serious problem of shear-locking for the thin plate, even if reduced/selected integration is applied for the element. However, the difficulty of constructing a simple and locking-free triangular plate element is effectively solved in the current MTPF by means of the definition of the new incompatible approximation in Eq. ([1](#)), which is independent of the nodes and triangular element shape. Furthermore, it is noted that regular full integration can be applied to make the element MTPF valid for the thin plate for the computation of Eq. ([25](#)), which differs from the work of Cai and Zhu ([2017a](#)) and others using reduced/selected integration for the shear term. The following numerical examples indicate that the current MTPF exhibits a highly effective convergence rate for both thick and thin plates.

3 Crack tip analysis

For the convenience of implementing the VCCT, as shown in Fig. [4](#)b, point q_2, which is the nearest node along the extended line direction of $q_1 - q$, is temporarily moved to q_3 to cause $q_1 - q$ and $q - q_3$ to have an equal distance. The movement of $q_2 - q_3$ does not affect interpolation accuracy, because the approximation in Eq. ([1](#)) is meshless and independent of the element shape.
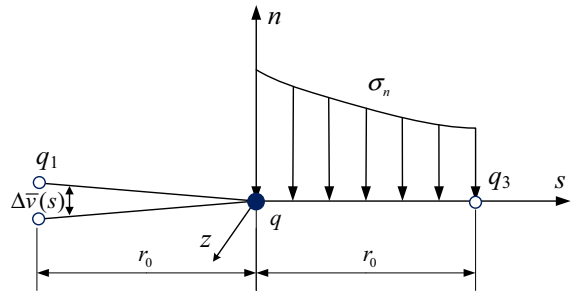
Fig. 5 Calculation of SIFs by VCCT

In the local coordinates (s, n, z) of Fig. [5](#), the relative displacements $[\Delta \bar{u}(s, z), \Delta \bar{v}(s, z), \Delta \bar{w}(s, z)]$ of $(-r_0, 0)$ to $(0, 0)$ in front of crack tip q and the stresses $[\tau_{ns}(s, z), \sigma_n(s, z), \tau_{nz}(s, z)]$ of $(0, 0)$ to $(r_0, 0)$ behind crack tip q can easily be calculated using Eqs. ([17](#)) and ([21](#)) for the thin layer. According to the VCCT (Rybicki and Kanninen [1977](#); Valvo [2015](#)), the energy release rate at crack tip q can be approximately calculated by

$$\begin{cases} G_{\mathrm{I}} \cong \frac{1}{2hr_0} \int_{-h/2}^{h/2} \int_0^{r_0} \sigma_n(s, z) \, \Delta \bar{v}(s - r_0, z) \, \mathrm{d}s \mathrm{d}z \\[2mm] G_{\mathrm{II}} \cong \frac{1}{2hr_0} \int_{-h/2}^{h/2} \int_0^{r_0} \tau_{ns}(s, z) \, \Delta \bar{u}(s - r_0, z) \, \mathrm{d}s \mathrm{d}z \\[2mm] G_{\mathrm{III}} \cong \frac{1}{2hr_0} \int_{-h/2}^{h/2} \int_0^{r_0} \tau_{nz}(s, z) \, \Delta \bar{w}(s - r_0, z) \, \mathrm{d}s \mathrm{d}z \end{cases} \tag{26}$$

where G_{I} is the energy release rate of crack mode I, G_{II} that of crack mode II, and G_{III} is that of crack mode III.

The SIFs for the Reissner–Mindlin plate are defined as:

$$\begin{cases} K_1 = \lim_{r \to 0} \sqrt{2\pi r}\, \sigma_\theta\,(r, 0, h/2) \\ K_2 = \lim_{r \to 0} \sqrt{2\pi r}\, \tau_{r\theta}\,(r, 0, h/2) \\ K_3 = \lim_{r \to 0} \sqrt{2\pi r}\, \tau_{\theta z}\,(r, 0, 0) \end{cases} \quad (27)$$

where r, θ are the local polar coordinates around crack tip q. The SIFs can be computed by means of the relations between the energy release rate and SIFs for the Reissner–Mindlin plate theory, for example, $K_1 = \sqrt{3EG_I}$ (Dirgantara and Aliabadi 2000).

It is observed that the proposed method contains a very simple formula that avoids using of singular integrations due to the local enrichment basis capturing the stress singularity around the crack tip, and prevents the relatively complicated J-integral for the crack modeling of plate bending problems in the previous popular methods. To the best of our knowledge, the proposed MTPF should be the simplest element for calculating the SIFs of the cracked thick–thin plates at this stage.

4 Numerical examples

In this section, several problems are solved in order to demonstrate the performance of the current element MTPF for the thick-to-thin plates.

4.1 Simply supported square plate under uniform load

A simply supported square plate under uniform load q is considered for linear elastic analysis. The plate side length and thickness are L and h, respectively. A quarter of the plate is modeled based on symmetry, as shown in Fig. 6. The $n \times n$ regular mesh in Fig. 7 and irregular mesh in Fig. 8 are employed for the convergence studies. This example is also solved by the MTP9 with the linear shape function and reduced/selected integration in Cai and Zhu (2017a), but here it is used for the purpose of testing the performance of the current MTPF without using reduced integration for the shear energy term.

In the following numerical examples, seven quadrature points for each triangular element (Cowper 1973) and three Gauss quadrature points for each fictitious layer are used for the MTPF integration using the quadratic shape function in Eq. (3). Furthermore, 12 quadrature points for each triangular element (Cowper 1973) and four Gauss quadrature points for each ficti-
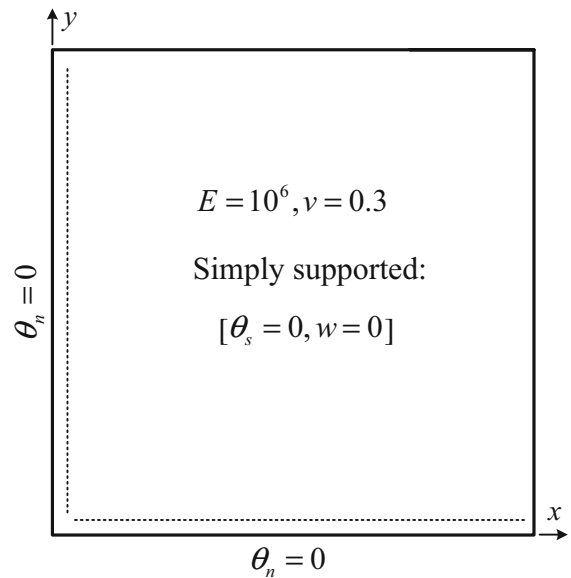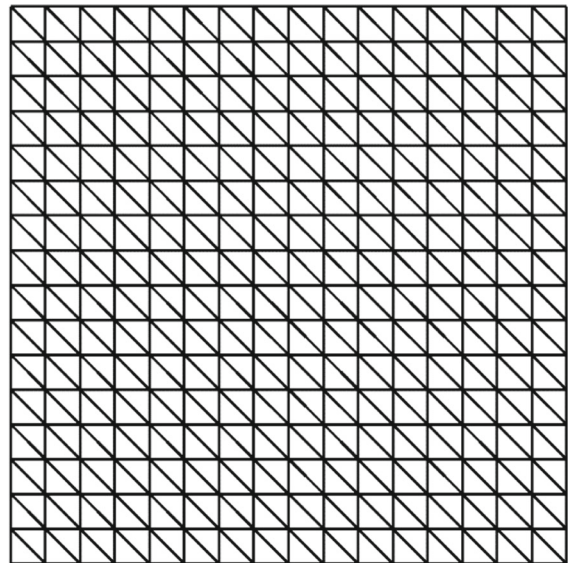

Fig. 6 Model of square plate

Fig. 7 Typical regular mesh (16×16) for square plate

tious layer are used for the MTPF integration using the cubic shape function in Eq. (4).

Tables 1 and 2 list the results of the dimensionless central displacement w_0 ($\times qL^4/100D_0$) for the simply supported plate with the quadratic and the cubic shape functions, respectively. The results listed in Tables 1 and 2 indicate that the current MTPF with the quadratic shape function is free from shear locking with an aspect
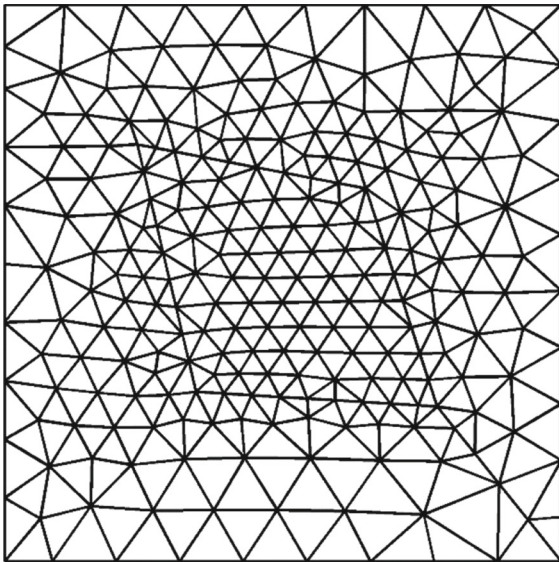
Fig. 8 Irregular mesh with 460 elements for square plate

Table 3 Number of quadrature points for reduced/selected integration of plate element

Shape function	Triangular element	Fictitious layer (bending term)	Fictitious layer (shear term)
Quadratic	4	3	2
Cubic	7	4	3

for the thick-to-thin plates, and is insensitive to element distortions of the irregular mesh in Fig. 8.

Similar to the MTP9 in Cai and Zhu (2017a), reduced/selected integration can be used to solve the problem of shear locking in the current plate element exploiting the higher-order displacement functions. Table 3 lists the number of quadrature points for reduced/selected integration of the plate element. Table 4 provides the central deflection of the simply supported square plate using reduced/selected integration and the regular mesh of 16×16. It can be seen that, although it is not necessary for practical engineering, the current plate element with reduced/selected integration exhibits effective performance for thick-to-thin plates (locking-free to the thin limit of $h/L = 0.0001$for both the quadratic and cubic shape functions).

Because the element MTPF with the cubic shape function exhibits an improved convergence rate and overall superior performance to that of the quadratic

ratio of $h/L \geq 0.005$, while the MTPF with the cubic shape function is locking-free to the thin limit of $h/L = 0.0001$. In general, from a practical viewpoint, the current MTPF with different shape function orders, which is locking-free at least for $h/L \geq 0.005$, is sufficient for the analyses of various thick–thin plate types in practical engineering. Tables 1 and 2 also illustrate that the present MTPF exhibits satisfactory results

Table 1 Central deflection for simply supported square plate with quadratic shape function

h/L	0.001	0.005	0.01	0.10	0.15	0.20	0.25	0.30
MTPF (4×4)	0.3288	0.3571	0.3789	0.4263	0.4532	0.4902	0.5376	0.5956
MTPF (8×8)	0.3538	0.3967	0.4029	0.4273	0.4537	0.4905	0.5379	0.5958
MTPF (16×16)	0.3947	0.4054	0.4062	0.4274	0.4537	0.4905	0.5379	0.5958
MTPF (Fig. 8)	0.3998	0.4053	0.4060	0.4274	0.4537	0.4906	0.5379	0.5958
Exact	0.4064	0.4064	0.4064	0.4273	0.4536	0.4906	0.5379	0.5956

Table 2 Central deflection for simply supported square plate with cubic shape function

h/L	0.0001	0.001	0.01	0.10	0.15	0.20	0.25	0.30
MTPF (4×4)	0.4025	0.4032	0.4062	0.4274	0.4537	0.4905	0.5379	0.5958
MTPF (8×8)	0.4052	0.4061	0.4065	0.4274	0.4537	0.4906	0.5379	0.5958
MTPF (16×16)	0.4052	0.4063	0.4065	0.4274	0.4537	0.4905	0.5379	0.5958
MTPF (Fig. 8)	0.4062	0.4063	0.4066	0.4274	0.4537	0.4906	0.5379	0.5958
Exact	0.4064	0.4064	0.4064	0.4273	0.4536	0.4906	0.5379	0.5956

Table 4 Central deflection for simply supported square plate using reduced/selected integration

h/L	0.0001	0.001	0.01	0.10	0.15	0.20	0.25	0.30
MTPF (quadratic)	0.4045	0.4059	0.4067	0.4274	0.4537	0.4905	0.5379	0.5958
MTPF (cubic)	0.4049	0.4063	0.4065	0.4274	0.4537	0.4905	0.5379	0.5958
Exact	0.4064	0.4064	0.4064	0.4273	0.4536	0.4906	0.5379	0.5956

**Table 5** Convergence of central deflection for simply supported square plate with different width-to-length ratios

δ/l	0.1	0.01	0.001	0.0001	0.00001	0.000001	0.0000001
MTPF (4×4)	0.4793	0.4157	0.4072	0.4062	0.4061	0.4061	0.4061
MTPF (8×8)	0.4841	0.4159	0.4074	0.4065	0.4064	0.4064	0.4064
MTPF (16×16)	0.4897	0.4157	0.4074	0.4065	0.4065	0.4064	0.4065
Exact	0.4064						

shape function, only the cubic shape function is studied in the following numerical examples.

In order to test the effect of the width-to-length ratio δ/l of the fictitious thin layer, the convergence of the simply supported square plate central deflection with different values of δ/l and an aspect ratio of $h/L = 0.01$ is shown in Table 5, and the results indicate that the ratio δ/l has little effect on the MTPF accuracy when $\delta/l \leq 0.001$.
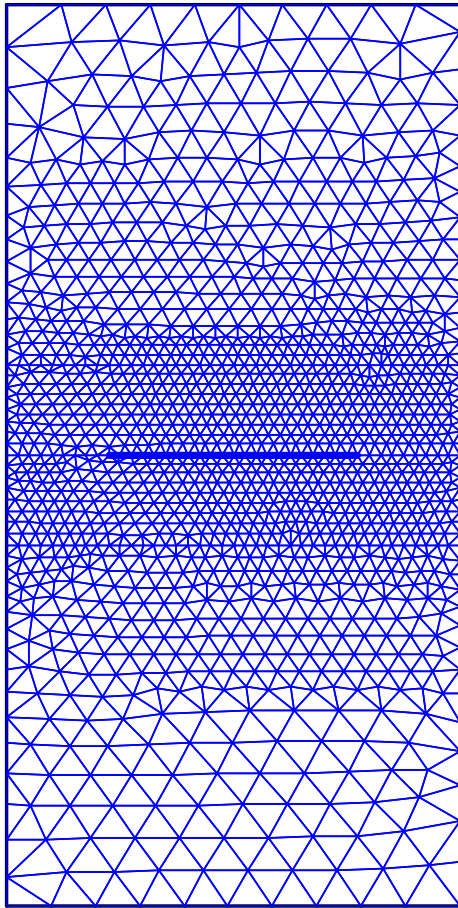
4.2 Rectangular plate with center crack

A rectangular plate with a center crack is analyzed, as illustrated in Fig. 9. The width and length of the plate are $2b = 1$m and $2c = 2$m, respectively, while the material properties are $E = 1.0\text{E}6$ MPa and $v = 0.3$. The crack size is $2a$, and the plate thickness is h. The two edges parallel to the crack are simply supported, and moment M is applied to these, while the other two edges are free. Divisions of 2728 and 7338 triangular elements are employed for the computation of the rectangular plate SIFs. Figure 10 illustrates a discrete model of the rectangular plate with 1421 triangular elements. The numerical results for different a/h are presented in Table 6, along with reference solutions for comparison (Tanaka et al. 2015; Boduroglu and Erdogan 1983), where the SIF is normalized by $F_1 = \frac{h^2 K_1}{6M\sqrt{\pi a}}$. It is observed that high-accuracy SIF solutions are obtained for the current element MTPF.
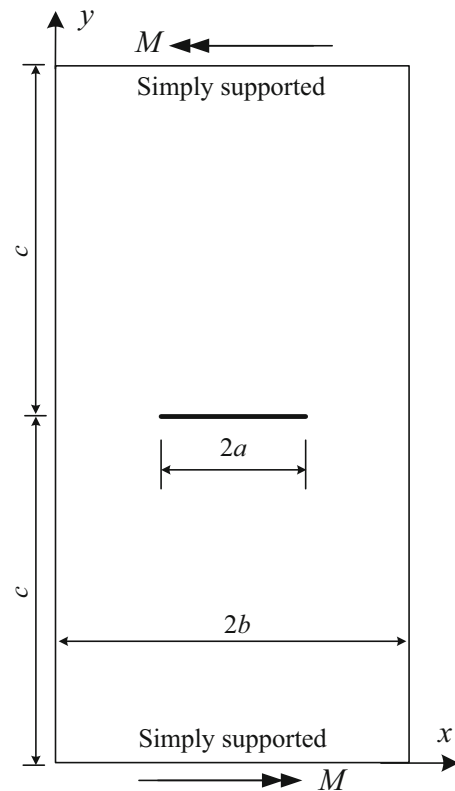
Fig. 9 Analysis model of center crack plate
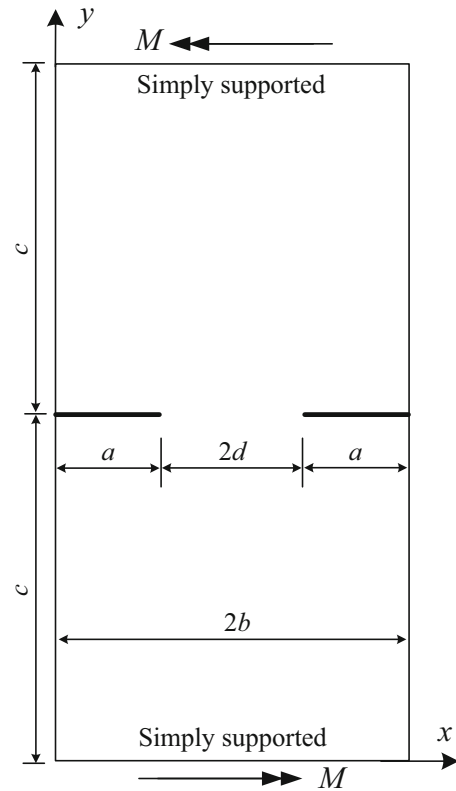
4.3 Rectangular plate with symmetric edge cracks

As illustrated in Fig. 11, symmetric edge cracks in a rectangular plate are analyzed. The boundary condi-

Fig. 10 Discrete model of center crack plate with 2728 triangular elements

Fig. 11 Analysis model of symmetric edge cracks in square plate

coincide with the reference solutions (Tanaka et al. 2015; Boduroglu and Erdogan 1983) in all cases.

4.4 Single crack emanating from hole

A single crack emanating from a hole in a finite rectangular plate is analyzed, as shown in Fig. 12. The width and length of the plate are $2b = 1$m and $2c = 2$m, respectively. The hole radius is $r = 0.05$m, the crack size is a, and the plate thickness is h, while the material properties are $E = 1.0E6$ MPa and $v = 0.3$. The

tions, geometry dimensions, and material properties are the same as those of the center crack problem described in Sect. 4.2. The crack size is a and the plate thickness is h. The discrete model with 2728 triangular elements shown in Fig. 10 is also employed for this problem. The numerical results for different d/b values are presented in Tables 7 and 8 for $b/h = 2.0$ and 10.0. As expected, the results obtained using the current method

Table 6 Normalized SIFs F_1 for center crack plate

a/h	0.8 (0.2/0.25)	1.0 (0.25/0.25)	4.0 (0.2/0.05)	5.0 (0.25/0.05)
MTPF (2728)	0.8637	0.9037	0.7275	0.7634
MTPF (7338)	0.8651	0.9057	0.7289	0.7651
Tanaka et al. (2015)	0.8683	0.9096	0.7287	0.7663
Boduroglu and Erdogan (1983)	0.8694	0.9094	0.7347	0.7702

Table 7 Normalized SIFs F_1 for symmetric edge crack problem ($b/h = 2.0$)

d/b	0.2	0.3	0.4	0.5	0.6
MTPF (2728)	1.3601	1.1128	0.9819	0.9066	0.8666
Tanaka et al. (2015)	1.3719	1.1201	0.9886	0.9110	0.8706
Boduroglu and Erdogan (1983)	1.3689	1.1174	0.9844	0.9086	0.8673

Table 8 Normalized SIFs F_1 for symmetric edge crack problem ($b/h = 10.0$)

d/b	0.2	0.3	0.4	0.5	0.6
MTPF (2728)	1.1076	0.9221	0.8255	0.7687	0.7359
Tanaka et al. (2015)	1.1144	0.9225	0.8246	0.7697	0.7377
Boduroglu and Erdogan (1983)	1.1140	0.9250	0.8268	0.7692	0.7351
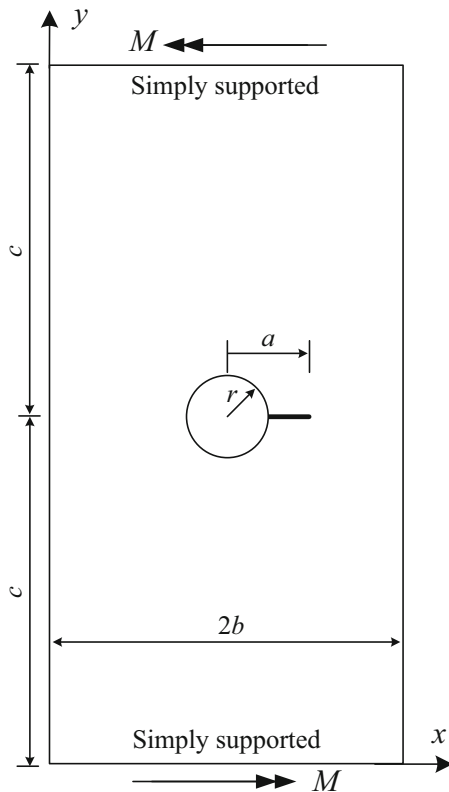
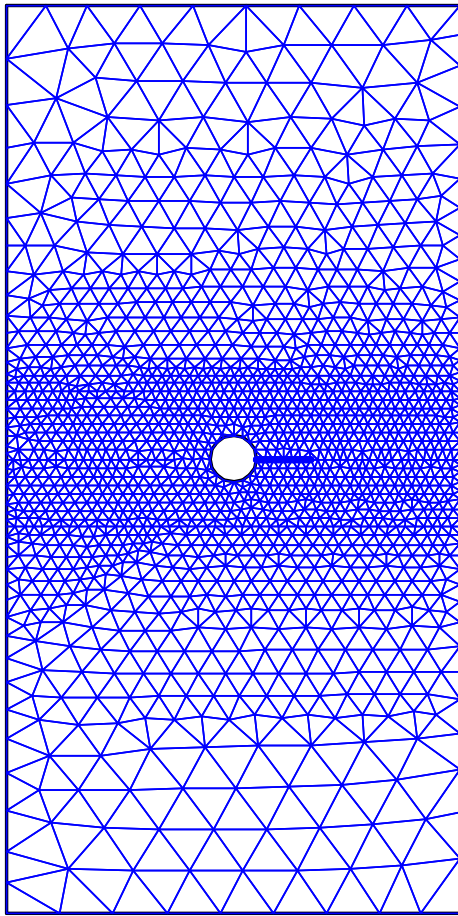**Fig. 12** Analysis model for a single crack emanating from a hole

two edges parallel to the crack are simply supported, and moment M is applied to these, while the other two edges are free. Different ratios of $a/b = 0.3$–0.8 are analyzed, and a division of 3076 triangular elements

is employed for the SIFs computation of the plate, as shown in Fig. 13. The numerical results for different b/h values are presented in Fig. 14, along with reference solutions for comparison (Dirgantara and Aliabadi 2002). It can be seen that the current results closely match the reference solutions.

5 Conclusions

In this work, a new locking-free element MTPF is developed for the analysis of cracked thick–thin plates. The proposed MTPF has the following characteristics:

(1) Without any numerical expediencies, such as reduced/selected integration, the use of assumed strain/stress, or the need for stabilization of the attendant zero energy modes, shear locking is completely eliminated to the thin limit of $h/L = 0.0001$ for the MTPF with a cubic shape function, which is very useful and applicable for the analyses of various hick-thin plate types in practical engineering.

(2) The MTPF has a very simple formulation as well as numerical implementation for including the transverse shear effects for thick plates. Furthermore, it exhibits an effective convergence rate, is insensitive to element distortions, and provides stable solutions for thick and thin plates.

(3) The element MTPF can conveniently compute the crack tip SIFs by using the VCCT, which has a very simple formula derivation and numerical implementation. Numerical examples indicate that the element MTPF maintains high accuracy in the cal-

Fig. 13 Discrete model for a single crack emanating from a hole
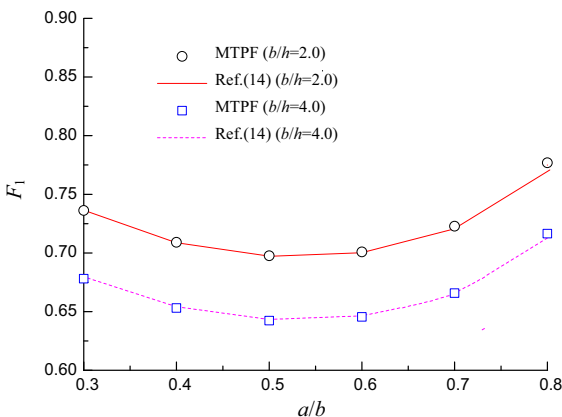
Fig. 14 Normalized SIFs for a single crack emanating from a hole

culation of crack tip SIFs for cracked thick–thin plates.

(4) The element MTPF uses a meshless approach and is independent of the nodes and triangle shape. Thus, similar to other meshless methods, the MTPF is easy and ready for automatic simulation of the failure process of a cracked plate along arbitrary directions by introducing an appropriate crack propagation criterion for the plates, and this will be the next work offered by the author.

References

Agnihotri SK, Parameswaran V (2016) Mixed-mode fracture of layered plates subjected to in-plane bending. Int J Fract 197:63–79

Ayad R, Dhatt G, Batoz JL (1998) A new hybrid-mixed variational approach for Reissner–Mindlin plates. The MiSP model. Int J Numer Methods Eng 42:1149–1179

Bathe KJ, Dvorkin EN (1985) A four-node plate bending element based on Mindlin/Reissner plate theory and a mixed interpolation. Int J Numer Methods Eng 21:367–383

Batoz JL, Lardeur P (1989) A discrete shear triangular nine d.o.f. element for the analysis of thick to very thin plates. Int J Numer Methods Eng 29:533–560

Batoz JL, Katili I (1992) On a simple triangular Reissner/Mindlin plate element based on incompatible modes and discrete constraints. Int J Numer Methods Eng 35:1603–1632

Bayesteh H, Mohammadi S (2011) XFEM fracture analysis of shells: The effect of crack tip enrichments. Comput Methods Appl Mech Eng 50:2793–2813

Bhardwaj G, Singh IV, Mishra BK, Bui TQ (2015) Numerical simulation of functionally graded cracked plates using NURBS based XIGA under different loads and boundary conditions. Compos Struct 126:347–59

Bhardwaj G, Singh IV, Mishra BK, Kumar V (2016) Numerical simulations of cracked plate using XIGA under different loads and boundary conditions. Mech Adv Mater Struct 23:704–714

Boduroglu H, Erdogan F (1983) Internal and edge cracks in a plate of finite width under bending. J Appl Mech Trans ASME 50:621–627

Brasile S (2008) An isostatic assumed stress triangular element for the Reissner–Mindlin plate-bending problem. Int J Numer Methods Eng 74:971–995

Cai YC, Zhu HH (2017a) A locking-free nine-dof triangular plate element based on a meshless approximation. Int J Numer Methods Eng 109:915–935

Cai YC, Zhu HH (2017b) Independent cover meshless method using a polynomial approximation. Int J Fract 203:63–80

Cen S, Shang Y (2015) Developments of Mindlin–Reissner plate elements. Math Probl Eng. https://doi.org/10.1155/2015/456740

Chang D, Kotousov A (2012) A strip yield model for two collinear cracks in plates of arbitrary thickness. Int J Fract 176:39–47

Chau-Dinh T, Zi G, Lee PS, Rabczuk T, Song JH (2012) Phantom-node method for shell models with arbitrary cracks. Comput Struct 92–93:242–56

Chen WJ, Cheung YK (2001) Refined 9-Dof triangular Mindlin plate elements. Int J Numer Methods Eng 51:1259–1281

Cowper GR (1973) Gaussian quadrature formulas for triangles. Int J Numer Methods Eng 7:405–408

Dirgantara T, Aliabadi MH (2000) Crack growth analysis of plates loaded by bending and tension using dual boundary element method. Int J Fract 105:27–47

Dirgantara T, Aliabadi MH (2002) Stress intensity factors for cracks in thin plates. Eng Fract Mech 69:1465–86

Katili I (1993) A new discrete Kirchhoff–Mindlin element based on Mindlin–Reissner plate theory and assumed shear strain fields–part I: an extended DKT element for thick-plate bending analysis. Int J Numer Methods Eng 36:1859–1883

Lim WK (2011) Determination of second-order term coefficients for the inclined crack in orthotropic plate using singular finite elements. Int J Fract 168:125–132

Liu P, Bui QT, Zhu D, Yu TT, Wang JW, Yin SH et al (2015) Buckling failure analysis of cracked functionally graded plates by a stabilized discrete shear gap extended 3-node triangular plate element. Compos B Eng 77:179–93

Mohammad M, Hossein MS, Reza N (2011) RKPM approach to elastic–plastic fracture mechanics with notes on particles distribution and discontinuity criteria. Comput Model Eng Sci 76:19–60

Nasirmanesh A, Mohammadi S (2015) XFEM buckling analysis of cracked composite plates. Comput Struct 131:333–343

Nguyen-Thoi T, Phung-Van P, Nguyen-Xuan H, Thai-Hoang C (2012) A cell based smoothed discrete shear gap method using triangular elements for static and free vibration analyses of Reissner–Mindlin plates. Int J Numer Methods Eng 91:705–741

Nguyen-Thoi T, Rabczuk T, Lam-Phat T, Ho-Huu V, Phung-Van P (2014) Free vibration analysis of cracked Mindlin plate using an extended cell-based smoothed discrete shear gap method (XCS-DSG3). Theor Appl Fract Mech 72:150–163

Nguyen-Thoi T, Nguyen-Thoi MH, Vo-Duy T, Nguyen-Minh N (2015) Development of the cell-based smoothed discrete shear gap plate element (CS-FEM-DSG3) using three-node triangles. Int J Comput Methods 12:1540015

Nguyen-Xuan H, Liu GR, Thai-Hoang C, Nguyen-Thoi T (2009) An edge based smoothed finite element method with stabilized discrete shear gap technique for analysis of Reissner–Mindlin plates. Comput Methods Appl Mech Eng 199:471–489

Phung-Van P, Nguyen-Thoi T, Tran VL, Nguyen-Xuan H (2013a) A cell-based smoothed discrete shear gap method (CS-DSG3) based on the C0-type higher-order shear deformation theory for static and free vibration analyses of functionally graded plates. Comput Mater Sci 79:857–872

Phung-Van P, Nguyen-Thoi T, Le-Dinh T, Nguyen-Xuan H (2013b) Static, free vibration analyses and dynamic control of composite plates integrated with piezoelectric sensors and actuators by the cell-based smoothed discrete shear gap method (CS-FEM-DSG3). Smart Mater Struct 22:095026

Rybicki EF, Kanninen MF (1977) A finite element calculation of stress intensity factors by a modified crack closure integral. Eng Fract Mech 9:931–938

Shi GH (1991) Manifold method of material analysis. In: Transactions of the ninth army conference on applied mathematics and computing, Minneapolis, Minnesota, pp 57–76

Shi GH (1993) Block system modeling by discontinuous deformation analysis. Computational Mechanics Publication, Boston

Tanaka S, Suzuki H, Sadamoto S, Imachi M, Bui TQ (2015) Analysis of cracked shear deformable plates by an effective meshfree plate formulation. Eng Fract Mech 144:142–157

Valvo PS (2015) A further step towards a physically consistent virtual crack closure technique. Int J Fract 192:235–244

Wang D, Peng H (2013) A Hermite reproducing kernel Galerkin meshfree approach for buckling analysis of thin plates. Comput Mech 51:1013–29

Yu TT, Bui QT, Liu P, Hirose S (2014) A stabilized discrete shear gap extended finite element for the analysis of cracked Reissner–Mindlin plate vibration problems involving distorted meshes. Int J Mech Mater Des 12:1–23